Nonequilibrium Synthesis and Assembly of Hybrid Inorganic−Protein Nanostructures Using an Engineered DNA Binding Protein

Haixia Dai,[†,‖] Woo-Seok Choe,[†,⊥] Corrine K. Thai,[†] Mehmet Sarikaya,[†,‡]
Beth A. Traxler,[§] François Baneyx,*[,†] and Daniel T. Schwartz*[,†,‡]

Contribution from the Departments of Chemical Engineering, Materials Science and Engineering, and Microbiology, University of Washington, Seattle, Washington 98195-1750

Received August 11, 2005; E-mail: dts@u.washington.edu; baneyx@u.washington.edu

Abstract: We show that a protein with no intrinsic inorganic synthesis activity can be endowed with the ability to control the formation of inorganic nanostructures under thermodynamically unfavorable (nonequilibrium) conditions, reproducing a key feature of biological hard-tissue growth and assembly. The nonequilibrium synthesis of Cu_2O nanoparticles is accomplished using an engineered derivative of the DNA-binding protein TraI in a room-temperature precursor electrolyte. The functional TraI derivative (TraIi1753::CN225) is engineered to possess a cysteine-constrained 12-residue Cu_2O binding sequence, designated CN225, that is inserted into a permissive site in TraI. When TraIi1753::CN225 is included in the precursor electrolyte, stable Cu_2O nanoparticles form, even though the concentrations of $[Cu^+]$ and $[OH^-]$ are at 5% of the solubility product (K_{sp,Cu_2O}). Negative control experiments verify that Cu_2O formation is controlled by inclusion of the CN225 binding sequence. Transmission electron microscopy and electron diffraction reveal a core−shell structure for the nonequilibrium nanoparticles: a 2 nm Cu_2O core is surrounded by an adsorbed protein shell. Quantitative protein adsorption studies show that the unexpected stability of Cu_2O is imparted by the nanomolar surface binding affinity of TraIi1753::CN225 for Cu_2O ($K_d = 1.2 \times 10^{-8}$ M), which provides favorable interfacial energetics (−45 kJ/mol) for the core−shell configuration. The protein shell retains the DNA-binding traits of TraI, as evidenced by the spontaneous organization of nanoparticles onto circular double-stranded DNA.

Introduction

Solution-based processing of inorganic materials is a highly refined art, where control of particle size, composition, and structure is guided by an understanding of electrochemical equilibria, nucleation processes, and colloid science.[1−4] Nevertheless, nature's ability to form both equilibrium solids (predicted by solution thermodynamics) as well as nonequilibrium solids (unexpected based on solution thermodynamics) is largely unmatched in the laboratory.[5−8] For example, marine organisms can grow calcium carbonate shells from seawater that is supersaturated in precursor reagents,[6] but they are also capable of synthesizing silica despite the fact that seawater is subsaturated in silicic acid precursors.[7] The realization that mineralizing proteins such as silicateins and silaffins are responsible for the growth and stabilization of silica,[9,10] and that other polypeptides are involved in the nucleation and assembly of a variety of hard and soft tissues, has opened new avenues of research in biomimetic materials design. Because natural mineralizing proteins are limited to the regeneration of the inorganic that they are associated with, much work has been directed at using combinatorial techniques to isolate short polypeptides or nucleic acids that bind inorganic compounds of engineering interest.[11,12] In recent years, phage display (PhD) and cell surface display (CSD) techniques have been used to identify inorganic binding polypeptides (7−15 amino acids) for a number of different materials, including semiconductors, metals, and metal oxides.[13−18]

† Department of Chemical Engineering.
‡ Department of Materials Science and Engineering.
§ Department of Microbiology.
‖ Current address: Cambrios Technologies Corp., 2450 Bayshore Parkway, Mountain View, CA 94043.
⊥ Current address: Department of Chemical Engineering, Sungkyunkwan University, Suwon, Korea 440-746.

(1) Sugimoto, T. *Fine particles: Synthesis, characterizaation, and mechanisms of growth*; Marcel Dekker: New York, 2000.
(2) Penner, R. M. *Acc. Chem. Res.* **2000**, *33*, 78−86.
(3) Switzer, J. A.; Kothari, H. M.; Poizot, P.; Nakanishi, S.; Bohannan, E. W. *Nature* **2003**, *425*, 490−493.
(4) Switzer, J. A.; Hung, C. J.; Huang, L. Y.; Switzer, E. R.; Kammler, D. R.; Golden, T. D.; Bohannan, E. W. *J. Am. Chem. Soc.* **1998**, *120*, 3530−3531.
(5) Schrier, R. W. *Renal and Electrolyte Disorders*, 6th ed.; Lippincott Williams & Wilkins: Philadelphia, 2003.
(6) Broecker, W. S.; Takahashi, T. *Deep-Sea Res.* **1977**, *25*, 65−95.
(7) McManus, J.; Hammond, D. E.; Berelson, W. M.; Kilgore, T. E.; Demaster, D. J.; Ragueneau, O. G.; Collier, R. W. *Deep-Sea Res., Part II* **1995**, *42*, 871−903.
(8) Kawahara, H. *J. Biosci. Bioeng.* **2002**, *94*, 492−496.

(9) Cha, J. N.; Shimizu, K.; Zhou, Y.; Christiansen, S. C.; Chmelka, B. F.; Stucky, G. D.; Morse, D. E. *Proc. Natl. Acad. Sci. U.S.A.* **1999**, *96*, 361−365.
(10) Kroger, N.; Deutzmann, R.; Sumper, M. *Science* **1999**, *286*, 1129−1132.
(11) Sarikaya, M.; Tamerler, C.; Jen, A. K. Y.; Schulten, K.; Baneyx, F. *Nat. Mater.* **2003**, *2*, 577−585.
(12) Sarikaya, M.; Tamerler, C.; Schwartz, D. T.; Baneyx, F. *Annu. Rev. Mater. Res.* **2004**, *34*, 373−408.
(13) (a) Brown, S. *Proc. Natl. Acad. Sci. U.S.A.* **1992**, *89*, 8651−8655. (b) Brown, S. *Nat. Biotechnol.* **1997**, *15*, 269−272.

Some of these molecules have shown an ability to catalyze,[9,19] nucleate,[18,20] organize,[16,21] and colloidally stabilize[22] inorganic solids, providing control of crystal form, shape, and solution dispersion. However, nucleation and growth of a nonequilibrium phase has not been demonstrated.

Cu_2O, a semiconductor that displays multiple excitons in the visible spectrum, is an excellent model material for studying protein-induced nonequilibrium phases, in part because we have previously identified several strong Cu_2O binding dodecapeptides,[23,24] but largely because the thermodynamics of phase formation in the copper−water−chloride systems is very well established.[25−27] Here, we report that the insertion of a disulfide-constrained Cu_2O binding dodecapeptide (denoted CN225) into a DNA binding protein (TraIi1753) endows the protein with an ability to grow stable Cu_2O nanoparticles under thermodynamically unfavorable conditions. Moreover, this functional TraI derivative retains its DNA binding ability and is able to assemble the resulting Cu_2O nanoparticles using DNA as a scaffold.

Experimental Section

TraI Insertion Mutagenesis and Permissive Site Identification. To isolate permissive site mutations in TraI protein, the *traI* gene was cloned onto the vector pTrc99A (Amersham Pharmacia) and the resulting plasmid was subjected to Tn*lacZ*/in mutagenesis, as previously described.[28] One of the isolated mutants had a 31-codon insertion into *traI* codon 1753 (with a unique *Bam*HI site). The pTrc99A derivative encoding this *traI* gene with 31-codon insertion was named p99I::i1753. The resulting TraI protein that contains a 31-residue insertion after the 1753rd amino acid was named TraIi1753 (see Table 1).

Genetic Engineering of a Cu_2O Binding Peptide into TraI Protein. To insert the Cu_2O-binding peptide CN225 into the identified permissive site of TraIi1753, two complementary 5′-phosphorylated oligonucleotides encoding a codon-optimized version of the CN225 dodecamer flanked by Cys-Gly-Pro and Gly-Pro-Cys tripeptides (Cys-Gly-Pro-Arg-His-Thr-Asp-Gly-Leu-Arg-Arg-Ile-Ala-Ala-Arg-Gly-Pro-Cys) and specifying *Bam*HI 5′ overhangs were purchased from Invitrogen. The oligonucleotides (5′GATCAGTGTGGTCCACGTCAT-ACCGATGGTCTGCGTCGTATTGCGGCGCGTGGTCCATGT3′ and 5′GATCACATGGACCACGCGCCGCAATACGACGCAGACCAT-

(14) (a) Sano, K.-I.; Shiba, K. *J. Am. Chem. Soc.* **2003**, *125*, 14234−14235. (b) Sano, K.-I.; Sasaki, H.; Shiba, K. *Langmuir* **2005**, *21*, 3090−3095.
(15) Kjaergaard, K.; Sorensen, J. K.; Schembri, M. A.; Klemm, P. *Appl. Environ. Microbiol.* **2000**, *66*, 10−14.
(16) Whaley, S. R.; English, D. S.; Hu, E. L.; Barbara, P. F.; Belcher, A. M. *Nature* **2000**, *405*, 665−668.
(17) Lee, S. W.; Mao, C. B.; Flynn, C. E.; Belcher, A. M. *Science* **2002**, *296*, 892−895.
(18) Naik, R. R.; Brott, L. L.; Clarson, S. J.; Stone, M. O. *J. Nanosci. Nanotechnol.* **2002**, *2*, 95−100.
(19) Gugliotti, L. A.; Feldheim, D. L.; Eaton, B. E. *Science* **2004**, *304*, 850−852.
(20) (a) Kramer, R. M.; Li, C.; Carter, D. C.; Stone, M. O.; Naik, R. R. *J. Am. Chem. Soc.* **2004**, *126*, 13282−13286. (b) Naik, R. R.; Stringer, S. J.; Agarwal, G.; Jones, S. E.; Stone, M. O. *Nat. Mater.* **2002**, *1*, 169−172. (c) Brown, S.; Sarikaya, M.; Johnson, E. *J. Mol. Biol.* **2000**, *299*, 725−735.
(21) (a) McMillan, R. A.; Howard, J.; Zaluzec, N. J.; Kagawa, H. K.; Mogul, R.; Li, Y.-F.; Paavola, C. D.; Trent, J. D. *J. Am. Chem. Soc.* **2005**, *127*, 2800−2801. (b) Mao, C. B.; Flynn, C. E.; Hayhurst, A.; Sweeney, R.; Qi, J. F.; Georgiou, G.; Iverson, B.; Belcher, A. M. *Proc. Natl. Acad. Sci. U.S.A.* **2003**, *100*, 6946−6951.
(22) Levy, R.; Thanh, N. T. K.; Doty, C.; Hussain, I.; Nichols, R. J.; Schiffrin, D. J.; Brust, M.; Fernig, D. G. *J. Am. Chem. Soc.* **2004**, *126*, 10076−10084.
(23) Dai, H.; Thai, C. K.; Sarikaya, M.; Baneyx, F.; Schwartz, D. T. *Langmuir* **2004**, *20*, 3483−3486.
(24) Thai, C. K.; Dai, H.; Sastry, M. S. R.; Sarikaya, M.; Schwartz, D. T.; Baneyx, F. *Biotechnol. Bioeng.* **2004**, *87*, 129−137.
(25) Muylder, J. V.; Zoubouv, N. D.; Poubaix, M. *Rapp. Tech.* **1961**, 1−23.
(26) Ji, J.; Cooper, W. C. *J. Appl. Electrochem.* **1990**, *20*, 818−825.
(27) De Zoubov, N.; Vanleugenhaghe, C.; Pourbaix, M. *Atlas of electrochemical equilibria in aqueous solution, section 14.1*; Pergamon Press: New York, 1966.
(28) Manoil, C.; Bailey, J. *J. Mol. Biol.* **1997**, *267*, 250−263.

Table 1. Schematic Illustration of the Peptides and Proteins Used in This Study[a]

Peptides and proteins (aa number or sequence)	Schematic of construct
CN225 (RHTDGLRRIAAR)	
TraI (1756aa)	
TraIi1753 (1787aa)	
TraIi1753::CN225 (1805aa)	RHTDGLRRIAAR S—S

[a] The left column gives the designated name and amino acid (aa) sequence or number for the various molecules. The right column shows a linearized schematic of the corresponding materials (lengths not to scale). The Cu_2O binding dodecapeptide CN225 is denoted by a short red ribbon, and native TraI protein is a long blue ribbon. The control TraI, TraIi1753, contains a 31-residue permissive insertion (green ribbon) after the 1753rd amino acid. The functional TraI derivative, TraIi1753::CN225, has disulfide constrained CN225 inserted within TraIi1753.

CGGTATGACGTGGACCACACT-3′) were resuspended in double deionized water (ddH$_2$O) to a final concentration of 200 μM. Aliquots (10 μL) were supplemented with an equal volume of 2X annealing buffer (80 mM Tris-HCl, pH 8.0, 20 mM MgCl$_2$, 100 mM NaCl), mixed, and held at 99 °C for 10 min. Hybridization was allowed to proceed by gradually cooling the mixture to 23 °C by unplugging the heating block. The resulting double-stranded DNA was purified using the Qiagen PCR purification kit. Plasmid p99I::i1753 was linearized by *Bam*HI digestion and dephosphorylated with shrimp alkaline phosphatase (Roche). Double-stranded oligonucleotides were mixed at a 3:1 or 15:1 molar excess with the linearized backbone followed by overnight ligation at 16 °C. The ligation mixture was subjected to *Bam*HI digestion to eliminate religated p99I::i1753, and the DNA was introduced into electrocompetent *E. coli* Top10 by electroporation. Individual transformants obtained after overnight incubation at 37 °C onto LB-agar plates supplemented with 100 μg/mL carbenicillin were grown in liquid medium, and plasmid DNA was extracted using the Qiagen kit. The resulting plasmids were screened by double digestion with *Bam*HI and *Nde*I. Because the *Bam*HI palindrome is destroyed during the insertion process, clones yielding a single 9.6 kbp band were subjected to sequencing using primer 5′GACTCTTATACACAAG-TAGCGTC3′, which hybridizes 5′ of the *Bam*HI site in the 31-codon scar left upon transposon excision. A plasmid containing the proper CN225 insert, p99I::i1753::CN225, was selected for subsequent work. The corresponding protein was named TraIi1753::CN225 (see Table 1).

The two mutant proteins, TraIi1753 and TraIi1753::CN225, were compared to wild-type TraI in a conjugation assay. An F′Δ*traI* donor strain was proficient for plasmid transfer to a recipient strain in the presence of the pTrc99A plasmid derivatives carrying the *traI*[+], *traIi1753*, and *traIi1753::CN225* alleles, indicating that the essential biological activities (helicase and relaxase) of the encoded proteins were intact.

TraIi1753 and TraIi1753::CN225 Protein Purification. CAW400 (*traI*) cells harboring either plasmid p99I::i1753 or p99I::i1753::CN225 were grown at 37 °C in 250 mL of LB medium supplemented with 100 μg/mL carbenicillin. Mid-exponential phase cells ($A_{600} \approx 0.4$) were treated with 1 mM IPTG to induce the *tra* promoter, and TraI variants were allowed to accumulate for 3 h. Cells were sedimented by centrifugation at 8000g for 15 min, washed with 10 mL of 50 mM potassium phosphate monobasic, pH 6.5, and resuspended into 5 mL of 50 mM Tris-HCl, pH 7.6, 10 mM EDTA, 0.1% Triton X100 supplemented with 0.1 mg/mL lysozyme, and 40 μg/mL PMSF. After

two cycles of freezing–thawing, the lysate was supplemented with $MgCl_2$ (to 1 mM final concentration), 5 μL of Dnase I (Boehringer-Mannheim) and held at room temperature until the viscosity had decreased. TraI-rich fractions were recovered by ammonium sulfate precipitation from a 30–40% saturation cut, resuspended into 3 mL of buffer A (20 mM Tris-HCl, pH 7.5, 0.1 mM EDTA, 10% glycerol), and dialyzed overnight against 2 L of the same buffer. Proteins were loaded on a DEAE Sephacel column (Sigma) equilibrated in buffer A and developed at 0.4 mL/min with a NaCl gradient. Fractions eluting at ~200 mM NaCl were pooled, dialyzed against buffer A, and loaded onto a Heparin agarose column (Sigma) equilibrated in buffer A supplemented with 50 mM NaCl. The column was developed at a 0.4 mL/min flow rate with a NaCl gradient in buffer A, and purified TraI was recovered from the 300–400 mM NaCl fractions. The protein was dialyzed against buffer A and stored at −80 °C before use. Protein concentrations were determined using the Coomassie dye-binding protein assay kit (Sigma).

TraI Adsorption Analysis. TraI adsorption on Cu_2O was characterized using an electrochemical quartz crystal microbalance (EQCN-700, ELCHEMA) with 10.0 MHz AT-cut quartz crystals coated with a uniform film of electrodeposited Cu_2O. Quartz crystal microbalance (QCM) methods have been widely used to study protein adsorption processes in recent years.[29–37] QCM is based on the change in the resonant oscillation frequency of a piezoelectric quartz crystal upon mass loading and is capable of detecting fractional monolayer mass changes on the order of 0.01 ng.

All gold-coated quartz crystals were cleaned in Piranha solution (30% H_2O_2:98% H_2SO_4 = 1:2) prior to use. A thin layer of Cu_2O was electrochemically deposited on the gold surface in an electrolyte of 0.4 M $CuSO_4$, 3 M lactic acid, and 5 M NaOH at pH ≈ 9.0.[38] The deposition was at −410 mV versus a saturated calomel reference electrode (SCE) for about 15 min. Following deposition of the Cu_2O film, it was rinsed with phosphate buffer, and then 3 mL of the 100 mM ph 8.0 phosphate buffer was added to completely cover the Cu_2O surface. Raman spectroscopy confirmed that this buffer did not alter the composition of the cuprous oxide thin film. Frequency change on the crystal was monitored after buffer addition. When the baseline drift reached steady state, protein samples were injected and subsequent frequency changes were recorded.

Cu₂O Nanoparticle Synthesis and Assembly. Cu_2O precursor electrolyte synthesis and particle formation experiments occurred in an electrochemical cell with a 1 mL anode compartment that was separated from a 50 mL cathode compartment by a glass frit. The cathode compartment was filled with 1 M NaCl. To make the precursor analyte solution, 2 μm-filtered 1 M NaCl solution was added to the anode compartment with or without TraIi1753 (control protein) or TraIi1753::CN225 (functional protein). The anode and cathode were 1 cm² Cu metal foil. Before each experiment, the copper foil was rinsed with acid to remove the surface oxide layer, subsequently rinsed with distilled water, dried with a laboratory tissue, and immediately placed into solution. A Princeton Applied Research 273A potentiostat/

galvanostat was operated galvanostatically at 10 mA for 1 min, producing approximately 6 mM total cuprous ion (Cu^+) in the analyte, based on Faraday's law. The various analytes (with or without proteins) made in this way are the precursor solutions for particle formation. All solutions were maintained at ambient conditions. Most of the cuprous ion (Cu^+) in the precursor analyte was in the form of $CuCl_n^{1-n}$ ($n = 2, 3$)[25,26] although, as discussed below, different solid phases also formed depending on what, if any, protein additions were included in the precursor electrolyte.

To assemble Cu_2O nanoparticles on DNA, 40 μL of the precursor analyte solution made in the presence of 1.2×10^{-8} M TraIi1753::CN225 was mixed with 10 μL DNA solution (3×10^{-8} M ϕX174 RFII DNA, circular form, diluted 10-fold from stock solution). The DNA stock solution (New England BioLabs) was 1000 μg/mL (3×10^{-7} M) ϕX174 RFII DNA supplied in 10 mM Tris-HCl (pH 8.0) and 1 mM EDTA.

Transmission Electron Microscopy (TEM) and Selected Area Electron Diffraction (SAED). TEM samples were made by applying 40 μL of the particle containing solutions to a carbon-coated TEM grid for 10 min, followed by three repeated 1 min rinses with deionized water. Excess rinse solution was removed by capillary wicking with the corner of a laboratory tissue. TEM and SAED data were obtained using a Philips EM420 transmission electron microscope with an acceleration voltage of 120 kV for inorganic materials and 40 kV for DNA-related samples. The electron diffraction patterns were obtained at a nominal camera length of 950 mm using a selected area aperture of 1.3 μm in diameter.

Measurement of pH and Oxidation–Reduction Potential (ORP) of Analyte Precursor Solution. The ORP indicator electrode was a 5 mm Pt disk that was electrochemically cleaned in 1 M H_2SO_4 by repeated cycling of the potential between −325 and +1625 mV versus SCE at 100 mV/s prior to use. The Pt electrode was then rinsed with deionized water and immediately used to measure the ORP of the analyte solution. The solution pH was measured using a pH meter (pH/CON 510 series, Oakton, USA).

Results and Discussion

Coupling Cu₂O Binding Sequence to a DNA Binding Protein TraI. To explore the role of protein-mediated nucleation, growth, and assembly, we sought to endow the protein TraI (DNA helicase I), a 192-kDa *E. coli* F plasmid-encoded protein required for bacterial conjugative DNA transfer,[39] with high Cu_2O binding affinity. TraI has several desirable attributes for this task: preliminary studies showed that native protein does not interact with Cu_2O; it does not contain native cysteine residues and it binds both single- and double-stranded DNA, providing a route for hierarchical materials assembly using DNA as a scaffold.

The DNA binding protein TraI was endowed with Cu_2O binding properties by inserting the Cu_2O binding polypeptide CN225, previously identified by us,[23,24] into a permissive site of TraI. CN225 was specifically selected over 32 other Cu_2O binding sequences because it was the strongest binding polypeptide based on a cell adhesion assays, and it lacked cysteine residues, ruling out thiol-mediated metal center binding and favoring loop formation by oxidation of the flanking cysteine thiols. Transposon mutagenesis identified permissive sites in TraI that tolerate extraneous amino acids based on the lack of effect of 31 residue insertions on mutant protein folding and function.[28] There were 15 TraI permissive site insertion mutants identified. One such permissive site was found after the 1753rd residue of the native protein, yielding the TraIi1753 variant.

(29) Bonroy, K.; Friedt, J. M.; Frederix, F.; Laureyn, W.; Langerock, S.; Campitelli, A.; Sara, M.; Borghs, G.; Goddeeris, B.; Declerck, P. *Anal. Chem.* **2004**, *76*, 4299–4306.
(30) Stadler, H.; Mondon, M.; Ziegler, C. *Anal. Bioanal. Chem.* **2003**, *375*, 53–61.
(31) Tanaka, M.; Mochizuki, A.; Shiroya, T.; Motomura, T.; Shimura, K.; Onishi, M.; Okahata, Y. *Colloids Surf., A* **2002**, *203*, 195–204.
(32) Tanaka, M.; Mochizuki, A.; Motomura, T.; Shimura, K.; Onishi, M.; Okahata, Y. *Colloids Surf., A* **2001**, *193*, 145–152.
(33) Shen, D. Z.; Huang, M. H.; Chow, L. M.; Yang, M. S. *Sens. Actuators, B* **2001**, *77*, 664–670.
(34) Fant, C.; Sott, K.; Elwing, H.; Hook, F. *Biofouling* **2000**, *16*, 119–132.
(35) Saito, N.; Matsuda, T. *Mater. Sci. Eng., C* **1998**, *6*, 261–266.
(36) Janshoff, A.; Steinem, C.; Sieber, M.; elBaya, A.; Schmidt, M. A.; Galla, H. J. *Eur. Biophys. J. Biophys. Lett.* **1997**, *26*, 261–270.
(37) Rodahl, M.; Hook, F.; Krozer, A.; Brzezinski, P.; Kasemo, B. *Rev. Sci. Instrum.* **1995**, *66*, 3924–3930.
(38) Bohannan, E. W.; Shumsky, M. G.; Switzer, J. A. *Chem. Mater.* **1999**, *11*, 2289–2291.

(39) Traxler, B. A.; Minkley, E. G. *J. Mol. Biol.* **1988**, *204*, 205–209.
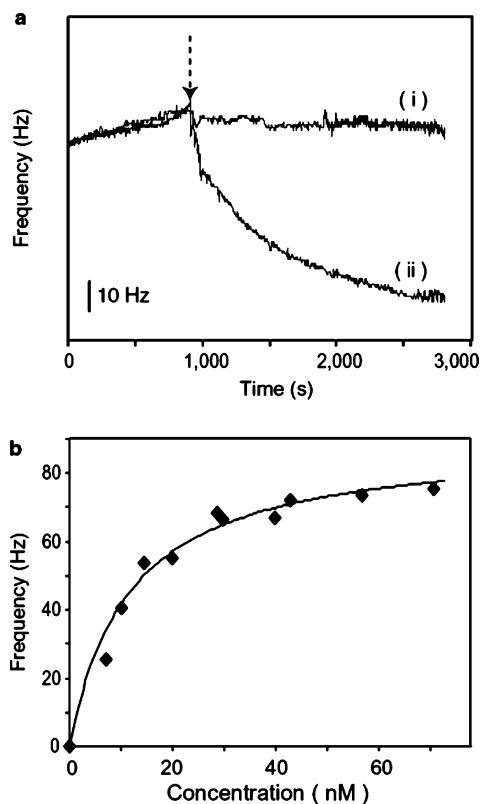
Figure 1. Adsorption properties of TraI variants on Cu_2O measured with an electrochemical quartz crystal microbalance. (a) Time course of the resonance frequency recorded in the presence of 15 nM of either TraIi1753 (trace i) or TraIi1753::CN225 (trace ii). The crystal was incubated for 15 min in the presence of 100 mM phosphate buffer before protein injection (vertical arrow). (b) Concentration dependence of the resonant frequency change for TraIi1753::CN225 adsorption on Cu_2O (♦) and best-fit to a Langmuir adsorption isotherm (−).

The Cu_2O binding dodecapeptide CN225 was then engineered within TraIi1753 along with flanking cysteine residues to form a disulfide-constrained Cu_2O-binding loop (see Experimental Section). Both the resulting protein, TraIi1753::CN225, and the negative control, TraIi1753, are functional in bacterial conjugative DNA transfer, which requires conservation of both relaxase and helicase activities. Table 1 schematically illustrates the characteristics of CN225 and all TraI derivatives discussed herein.

Characterization of TraI Protein Affinity for Cu_2O. Protein binding to Cu_2O was quantified by monitoring resonant frequency shifts for a Cu_2O-coated quartz crystal immersed in protein-containing phosphate buffer. Figure 1a shows the changes in resonant frequency that results from the injection of 1.5×10^{-8} M TraIi1753 (trace i) or TraIi1753::CN225 (trace ii) into the buffer. Before the injection of protein (denoted by the arrow), a small and predictable baseline drift is observed due to the slow dissolution of the Cu_2O film (the dissolution rate is 2 Å/h based on the Sauerbrey equation). No appreciable frequency change is observed after adding the control TraIi1753 (trace (i)), indicating negligible Cu_2O adsorption at this concentration. In contrast, injection of the same concentration of the Cu_2O-binding derivative, TraIi1753::CN225, induces a 55 Hz decline in frequency at long times (trace (ii)), indicating strong adsorption to the surface. TraIi1753 and TraIi1753::CN225 differ by 1% in amino acid sequence, but this small change gives rise to a large modulation in the surface

affinity of the molecule without destroying TraI function. Figure 1b shows measurements of TraIi1753::CN225 adsorption-induced frequency change for several different concentrations of protein. The magnitude of the resonant frequency change is seen to increase as the TraIi1753::CN225 concentration increases, up to 3×10^{-8} M, where a saturation of the adsorption is seen to produce a maximum frequency shift we denote Δf_{max}. Even though the frequency change cannot be easily translated directly into mass load for a large macromolecule like a protein, the assumption of linear response allows the experimental frequency change data to be fit to a Langmuir adsorption isotherm of the form $\Delta f = (\Delta f_{max} \times C)/(K_d + C)$, as represented by the smooth curve in Figure 1b. The fitting parameter K_d is the equilibrium dissociation constant, which is the protein concentration that produces 50% surface coverage. The model best-fit yields an equilibrium dissociation constant of $K_d = 1.2 \times 10^{-8}$ M, indicating that TraIi1753::CN225 has been successfully endowed with high binding affinity for Cu_2O. From previous work, we know that cysteine-constrained CN225 can also endow the host protein with binding selectivity for Cu_2O over other related compounds such as $Cu(OH)_2$.[23]

Nonequilibrium Cu_2O Nanoparticle Formation. The creation of a nanomolar binding affinity protein that is also selective to a target inorganic opens several opportunities for materials engineering. Here, we seek to use the well-characterized thermodynamic speciation of the $Cu-Cl-H_2O$ system as a foundation for exploring selective growth of a nonequilibrium solid phase. Under ambient conditions, the analyte precursor solution described in the Experimental Section (with no proteins) has an oxidation−reduction potential (ORP) of ∼370 mV versus NHE and a pH of 6.0, placing the electrolyte on the thermodynamic phase boundary between the inorganic solid $Cu_2Cl(OH)_3$ and the soluble $CuCl_n^{1-n}$ chloride complexes in solution.[25] Indeed, TEM imaging (Figure 2a) shows that ∼300 nm particles are present in solution, and their electron diffraction pattern (Figure 2a inset) matches that of $Cu_2Cl(OH)_3$. The thermodynamics of this electrolyte can be further explored by taking the same protein-free analyte precursor and elevating the pH to >7.0, at which point Cu_2O becomes the thermodynamically preferred inorganic solid phase;[25] the resulting Cu_2O precipitate is observed with the naked eye and was corroborated by Raman spectroscopy and electron diffraction. Cu_2O particles precipitated in this manner are highly polydispersed in size (not shown). In short, the protein-free analyte solution follows the expected thermodynamic patterns for solid formation, although one has little control over the particle size distribution when simply manipulating the pH to form Cu_2O.

To explore the role of protein-mediated nucleation and growth, we performed separate experiments using the functional protein TraIi1753::CN225 and control TraIi1753 in the precursor analyte solution. Supplementation of the analyte solution with 12 nM of control TraIi1753 led to the formation of crystalline particles that were smaller (Figure 2b, characteristic size 100−200 nm) and more abundant than those observed in protein-free solution (compare with Figure 2a). Nevertheless, the electron diffraction pattern (Figure 2b inset) showed (201), (220), (202), (231), and (203) rings characteristic of $Cu_2Cl(OH)_3$. Thus, control TraIi1753 behaves like a nonspecific contaminant by promoting nucleation of the thermodynamically expected solid.
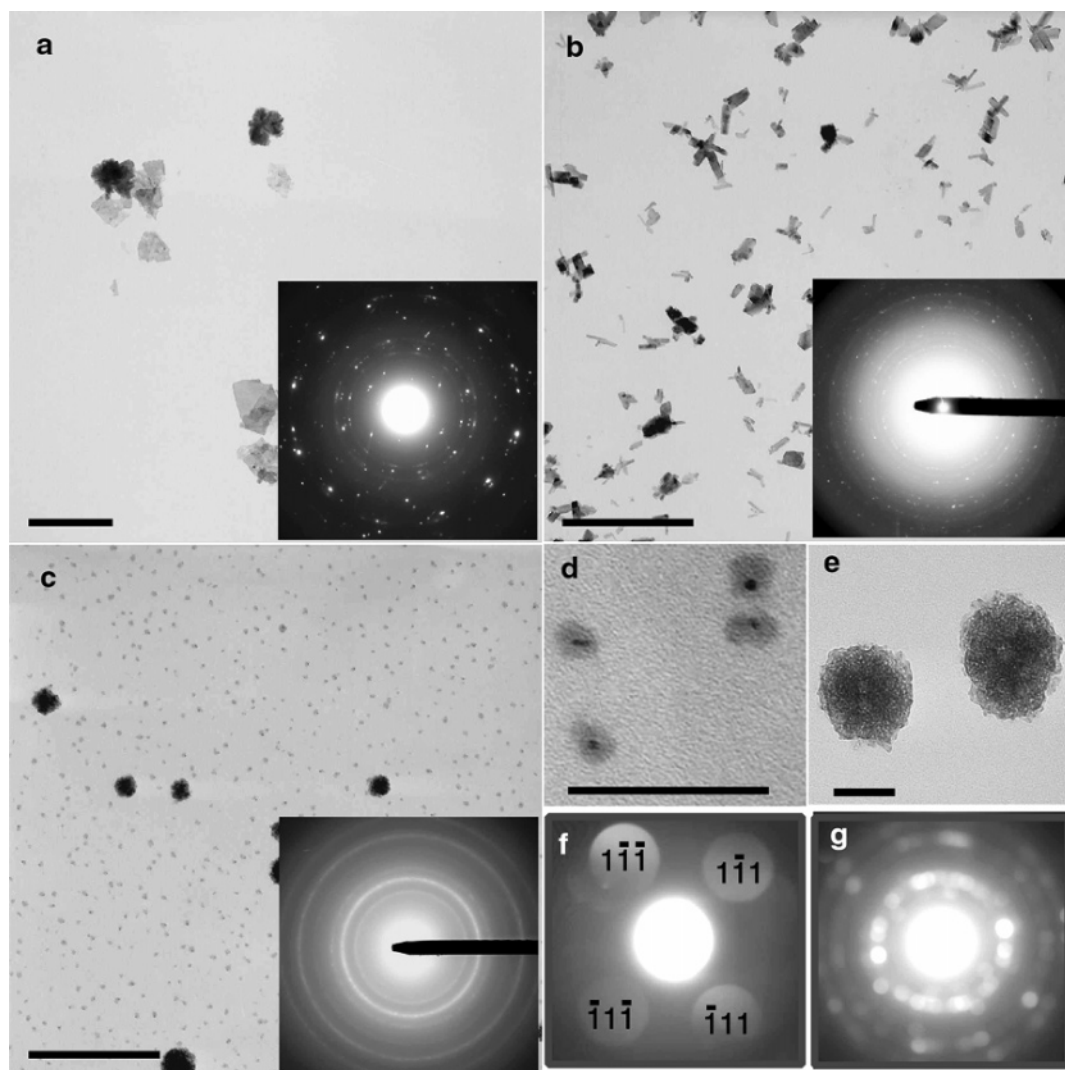
Figure 2. TEM images and selected area electron diffraction (SAED) patterns of particles formed in the analyte precursor solution: (a) without protein addition, (b) in the presence of 12 nM TraIi1753, and (c) in the presence of 12 nM TraIi1753::CN225. SAED from panels (a) and (b) indicate that the particles are $Cu_2Cl(OH)_3$, whereas the particles in (c) are Cu_2O. Higher magnification images from panel (c) show that the small individual particles (d) have a core–shell structure, whereas the larger particles (e) are agglomerated structures. Convergent beam electron diffraction patterns from an individual core–shell particle (f) and the larger agglomerated particles (g) indicate that both are Cu_2O. Scale bars are 500 nm in panels a, b, and c, and 100 nm in panels d and e.

When the above experiment was repeated with an identical 12 nM concentration of purified Cu_2O binding protein TraIi1753::CN225, the resulting particles were radically different in size and morphology than those seen previously. TEM showed uniformly distributed particles of 10 nm average diameter, as well as occasional ~100 nm clusters (Figure 2c). Higher resolution TEM imaging revealed that each small particle consisted of a ~2 nm dense core surrounded by a low-density outer region (Figure 2d) and that agglomeration of these core–shell particles was responsible for the formation of occasional large clusters (Figure 2e). Electron diffraction of selected areas (Figure 2c, inset) revealed concentric rings corresponding to the (110), (111), (200), (211), (220), and (310) lattice planes of cubic Cu_2O. The composition of an individual particle was confirmed with convergent beam electron diffraction, where one observes the {111} family of Cu_2O planes struck from a beam in the [110] direction (Figure 2f). Convergent beam electron diffraction (Figure 2g) of a larger cluster revealed the poly-crystalline nature of the multiparticle agglomerate, with clear rings from the (110), (111), (200), (211), (220), and (310) lattice

planes of Cu_2O. In short, the addition of 12 nM Cu_2O binding protein TraIi1753::CN225 altered the electrochemical equilibrium of the electrolyte, producing stable Cu_2O nanoparticles under thermodynamically unfavorable conditions.

The core–shell structure revealed in Figure 2d is comprised of a dense Cu_2O core surrounded by a low density adsorbed protein shell. The mechanism for driving the formation of a (nominally) soluble solid by adsorption of a selective, high affinity inorganic binding protein can be understood qualitatively from classical nucleation theory. At the pH and Cl^- concentrations of the electrolyte, the formation of soluble chloride complexes $CuCl_n^{1-n}$ in the analyte solution limits the free cuprous (Cu^+) and hydroxide concentrations to approximately 5% of the solubility product ($K_{sp} \approx 1.45 \times 10^{-15}$) for Cu_2O formation.[27] Even under these thermodynamically unfavorable conditions, nucleation rate theory suggests that Cu_2O can transiently nucleate, but then spontaneously redissolves because the electrolyte is subsaturated in the precursor ions (i.e., growth of the nascent Cu_2O nuclei would increase the Gibbs energy of the system).[40] Our ability to grow crystalline Cu_2O nanoparticles

from this electrolyte with the addition of nanomolar concentrations of TraIi1753::CN225, but not with control TraIi1753, indicates the central role of interfacial adsorption in selectively stabilizing nascent Cu_2O nuclei before they redissolve. Quantitatively, the equilibrium dissociation constant for TraIi1753::CN225 on Cu_2O is related to the Gibbs energy of adsorption by $\Delta G_{ads} = RT \ln(K_d)$. Using the value determined in Figure 1b, $K_d = 1.2 \times 10^{-8}$ M, shows that strong protein binding provides a stabilizing adsorption energy of $\Delta G_{ads} \approx -45$ kJ/mol. Because the CN225 polypeptide confers selectivity as well as strong binding to Cu_2O,[23] other nuclei do not derive the same energetic benefit from the presence of the functional protein. Thus, the binding of TraIi1753::CN225 to nominally soluble Cu_2O nuclei stabilizes the otherwise thermodynamically unfavorable solid by providing beneficial adsorption energy when Cu_2O−protein interfaces form. The control TraIi1753 does not possess these binding properties, so it acts as a nonspecific contaminant that simply reduces the kinetic barrier to nucleation without shifting the energetics of the final products.

The concentration of TraIi1753::CN225 in the analyte changes the monodispersity of the resulting Cu_2O nanoparticles; more large agglomerated particle clusters are obtained when the TraIi1753::CN225 concentration in the analyte is 8 nM, whereas large clusters are extremely rare when the protein concentration is raised to 40 nM (not shown).

Cu_2O Nanoparticle Assembly. In nature, mineralizing proteins not only nucleate and stabilize materials, but they also assemble and organize inorganic components into complex higher order structures. The DNA-binding traits of the TraI shell provide an opportunity to emulate this second function, if DNA binding activity is retained once the TraIi1753::CN225 is adsorbed on the nanoparticle surface. We assayed DNA-directed nanoparticle assembly using the double-stranded relaxed form II (RFII) DNA of bacteriophage ϕX174 that adopts a circular conformation when one of its two strands is nicked. The core−shell Cu_2O-TraIi1753::CN225 nanoparticles in analyte solution were mixed with the nicked DNA, and aliquots of the mixture were imaged by TEM. Figure 3 shows that the protein-coated Cu_2O nanoparticles spontaneously assembled onto the DNA, yielding smooth circular loops with evenly separated metal oxide nanoparticles (inset). Most of the nanoparticle decorated loops were ∼300 nm in circumference, which is about 1/6 of the expected contour length of ϕX174 RFII DNA (1800 nm). Such DNA condensation effects have been reported previously,[41] although it is not clear if the TraI DNA binding mechanism or other types of interactions are responsible. These proof-of-concept experiments made no effort to fully optimize nanostructure assembly, so individual core−shell particles and some incompletely decorated loops appear in Figure 3 (see arrow).

Conclusion

We have shown that the permissive insertion of a cysteine-constrained inorganic binding motif into the DNA-binding protein TraI endows it with nanomolar binding affinity for the inorganic while retaining its primary relaxase and helicase activities. The measured binding affinity of TraIi1753::CN225 for Cu_2O ($K_d = 1.2 \times 10^{-8}$ M) is outstanding even by biological
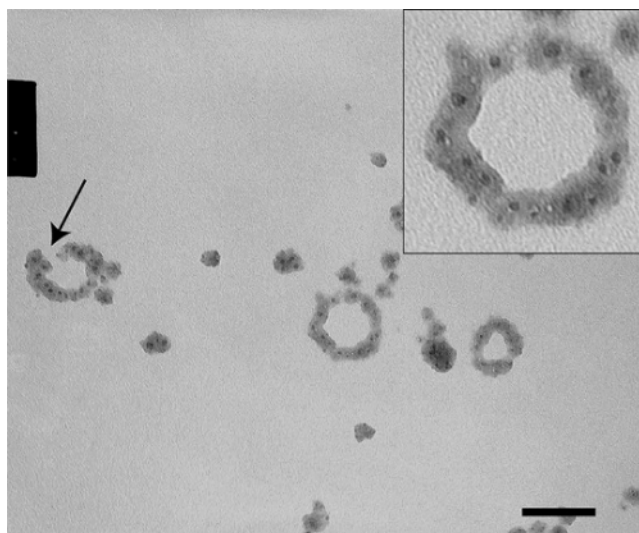
Figure 3. TEM images of Cu_2−TraIi1753::CN225 nanoparticles self-organized on circular ϕX174 RFII DNA. Nanoparticle loops are never observed in the absence of circular DNA additions. The arrow identifies an incompletely decorated loop. Scale bar: 100 nm.

standards; it is stronger than typical enzyme−substrate interactions ($K_d \approx 10^{-2}$–10^{-6} M) and is comparable to some tight antibody−antigen interactions (for example, *Staphylococcus aureus* protein A and the F_c fragment of antibodies has $K_d = 2 \times 10^{-8}$ M).[42] The inorganic binding traits of TraIi1753::CN225 are shown to exert extraordinary control over the aqueous synthesis of nonequilibrium nanoparticles with modest size polydispersity. Moreover, the resulting nanoparticles have a protein shell that retains biological functionality, providing a mechanism for organized self-assembly using DNA as a scaffold. In short, we have shown that a protein with no intrinsic inorganic synthesis activity can be endowed with the ability to control the formation and organization of inorganic nanostructures under thermodynamically unfavorable conditions, reproducing a key feature of biological hard-tissue growth and assembly.

There are several important bionanotechnology implications of this work. Here, a single permissive insertion was made in TraI, but there are 15 different permissive sites currently identified for this protein. Thus, we have already begun to insert different inorganic binding motifs into different permissive sites, in an effort to create molecular linkers that can connect and organize multiple nanoparticles (similar or dissimilar) into precisely spaced building blocks. In this work, we have found TraI to be a particularly salt-tolerant protein, so it placed few constraints on the electrolyte formulation used. Nonetheless, there is every reason to believe other proteins can be engineered to perform synthesis functions such as TraIi1753::CN225, but in even more complex multicomponent electrolytes (they do in nature). Ideally, a library of multifunctional inorganic binding proteins will be developed for use with a single complex electrolyte, allowing selective precipitation of different materials from a single pot. More sophisticated models of electrolyte speciation and greater attention to protein−electrolyte interactions will be needed to realize this goal. However, the power of the approach laid out here should grow exponentially as experience is gained mating diverse proteins with diverse

(40) Adamson, A. W. *Physical Chemistry of Surfaces*; Wiley: New York, 1990.
(41) Cassell, A. M.; Scrivens, W. A.; Tour, J. M. *Angew. Chem., Int. Ed.* **1998**, *37*, 1528−1531.

(42) Jonsson, S.; Kronvall, G. *Eur. J. Immunol.* **1974**, *4*, 29−33.

inorganic synthesis conditions, thereby helping to establish the rules for success and creating a new generation of functional materials and devices.